# Exotic $d$-Wave Superconducting State of Strongly Hole-Doped $K_xBa_{1-x}Fe_2As_2$

Ronny Thomale,[1] Christian Platt,[2] Werner Hanke,[2] Jiangping Hu,[3] and B. Andrei Bernevig[1]

[1]*Department of Physics, Princeton University, Princeton, New Jersey 08544, USA*
[2]*Institute for Theoretical Physics and Astrophysics, University of Würzburg, Am Hubland, D 97074 Würzburg, Germany*
[3]*Department of Physics, Purdue University, West Lafayette, Indiana 47907, USA*

(Received 20 January 2011; published 8 September 2011)

We investigate the superconducting phase in the $K_xBa_{1-x}Fe_2As_2$ 122 compounds from moderate to strong hole-doping regimes. Using the functional renormalization group, we show that, while the system develops a nodeless anisotropic $s^{\pm}$ order parameter in the moderately doped regime, gapping out the electron pockets at strong hole doping drives the system into a nodal $(\cos k_x + \cos k_y)(\cos k_x - \cos k_y)$ $d$-wave superconducting state. This is in accordance with recent experimental evidence from measurements on $KFe_2As_2$ which observe a nodal order parameter in the extreme doping regime. The magnetic instability is strongly suppressed.

DOI: 10.1103/PhysRevLett.107.117001 PACS numbers: 74.20.Mn, 74.20.Rp, 74.25.Jb

The most elementary questions in the field of iron-based superconductors, such as the symmetry of the order parameter in the superconducting (SC) state, are still under vivid debate. The complexities involve an intricate band structure, a diversity of different material compounds which exhibit sometimes contradictory behavior, and the proximity of various symmetry-broken phases. Because of best single-crystal quality, the most studied pnictide compounds belong to the 122 family such as $BaFe_2As_2$. Their crystal structure is tetragonal $I4/mmm$, where the Fe and As atoms arrange into layers; the intralayer hybridization is dominant, but, unlike other pnictide compounds such as the 1111 family, the interlayer hybridization is also important. Soon after their discovery [1], the 122 compounds have been synthesized not only with Ba as a substituent between the FeAs layers but also with K, Cs, and Sr. The SC transition temperatures achieved were up to 37 K [2].

The current theoretical opinion on the SC order parameter has converged on a nodeless $s^{\pm}$ order parameter that changes sign between the electron ($e$) pockets and hole ($h$) pockets. This order parameter comes out of both the strong- and the weak-coupling pictures of the iron-based superconductors [3–7] and owes its origin to the pnictide Fermi surface (FS) topology of $h$ pockets at the $\Gamma$ and $e$ pockets at the $X$ $(\pi, 0)/(0, \pi)$ point of the unfolded Brillouin zone. The dominant scattering contributions originate from $h$ pocket scattering at $\Gamma$ to $e$ pockets at $X$, yielding the $s^{\pm}$ SC order parameter for the doped case and the collinear antiferromagnetic phase in the undoped case. Detailed nesting properties of the pockets, the multiorbital character of the FS, and the presence or absence of a third $h$ pocket at $M$ $(\pi, \pi)$ in the unfolded Brillouin zone complicate this picture. For the 1111 compounds, it was shown that the absence of the $M$ $h$ pocket (whose Fermi level can be significantly tuned by the pnictogen height through replacing As by P) can modify the SC order parameter anisotropy from a nodeless to a nodal $s^{\pm}$ phase, which gives the correct material trend for As-P substitution in other pnictide families [7–9]. With small exceptions, the anisotropic extended $s$-wave scenario (and its extension to the nodal $s^{\pm}$) was consistent with experimental findings for most of the pnictide compounds [10–15].

It was realized at a very early stage that electron and hole doping can have qualitatively different effects in the pnictides [16]. Hole doping should increase the propensity to a nodeless ($s^{\pm}$) SC phase. The qualitative picture applies to both the 122 and the 1111 compounds: As the Fermi level is lowered, the $M$ $h$ pocket becomes more relevant and the $M \leftrightarrow X$ scattering adds to the $(\pi, 0)/(0, \pi)$ scattering from $\Gamma$ to $X$. As such, the anisotropy-driving scattering such as interelectron pocket scattering becomes less relevant, and it yields a nodeless, less anisotropic, and more stable $s^{\pm}$ [9,17]. This picture is qualitatively confirmed by experiments. While thermoelectric, transport, and specific heat measurement have been performed for $K_xBa_{1-x}Fe_2As_2$ from $x = 0$ to the strongly hole-doped case $x = 1$ [18–20], more detailed studies have previously focused on the optimally doped case $x = 0.4$ with $T_c = 37$ K, where all measurements such as penetration depth and thermal conductivity find indication for a moderately anisotropic nodeless gap [13,21–23]. Angle-resolved photoemission spectroscopy (ARPES) on doped $BaFe_2As_2$, likewise, finds a nodeless SC gap [24–26].

The experimental findings for the SC phase in $KFe_2As_2$ came as a surprise. Thermal conductivity [27,28], penetration depth [29], and NMR [30,31] provide clear indication for nodal SC. The critical temperature for $KFe_2As_2$ is at $T_c \sim 3$ K, an order of magnitude less than the optimally doped samples. ARPES measurements [32] show that the $e$ pockets have nearly vanished, while the $h$ pockets at the folded $\Gamma$ point are large and have a linear dimension close to $\pi/a$. In this Letter, we provide a detailed picture of how the SC phase evolves under hole doping in $K_xBa_{1-x}Fe_2As_2$ and find that the nodal phase observed for $x = 1$ is of the

 © 2011 American Physical Society

(extended) $d$-wave type. We use the functional renormalization group (FRG) to investigate how the SC form factor evolves under doping from nodeless anisotropic $s^{\pm}$ in the moderately hole-doped regime to a $d$ wave in the strongly hole-doped regime, where the $e$ pockets are assumed to be gapped out. The $d$-wave SC minimizes the on-pocket hole interaction energy. We find the critical divergence scale to be an order of magnitude lower than for the optimally doped $s^{\pm}$ scenario, which is consistent with experimental evidence.

We focus on studying $K_xBa_{1-x}Fe_2As_2$ starting at the optimally doped case around $x = 0.4$ and increasing the hole doping up to $KFe_2As_2$. We use an effective 5-band tight-binding model developed by Graser *et al.* [33] to describe the band structure of the 122-type iron-based superconductors [see Fig. 1]:

$$H_0 = \sum_{\boldsymbol{k},s} \sum_{a,b=1}^{5} c^{\dagger}_{\boldsymbol{k}as} K_{ab}(\boldsymbol{k}) c_{\boldsymbol{k}as}. \tag{1}$$

Here $c$'s denote electron annihilation operators, $a$ and $b$ the five Fe $d$ orbitals, $K$ the band matrix, and $s$ the spin index. As seen in Figs. 1 and 2, for moderate hole doping, the conventional five pocket scenario with $e$ pockets at $X(\pi, 0)$ and $M(\pi, \pi)$ emerges. For larger hole doping, the $e$ pockets vanish and only small disconnected lobe features are found around $X$ [Fig. 2(c)]. The kinetic model reduces to the effectively three $h$ pocket scenario shown in Fig. 2(c). Other details of the 122 band structure are currently still under debate, with unresolved questions about the FS topology at the $Z$ point in the three-dimensional Brillouin zone and the importance of integrating over the full range along $k_z$. However, as many of these details mostly affect the $e$ pocket anisotropies, they are irrelevant for our proposed SC mechanism: As we always consider a rather largely hole-doped regime, the $e$ pockets can be assumed relatively small—even disappearing in the most interesting case, i.e., that of full hole doping. We, therefore, particularize to the $k_z = 0$ cut of (1) in the following and also omit the lobe features at large hole doping within the RG calculations. To test our assumption of the irrelevance of the $k_z$ dispersion to our results, we have made several other cuts at different $k_z$ and confirmed that our results do not change qualitatively. We cannot ultimately exclude that the lobes may influence the system due to the fact that our Brillouin zone patching scheme is not fully adequate for such small Fermi surface features. Still, within our formalism, we find that the lobes are negligible in the RG flow.

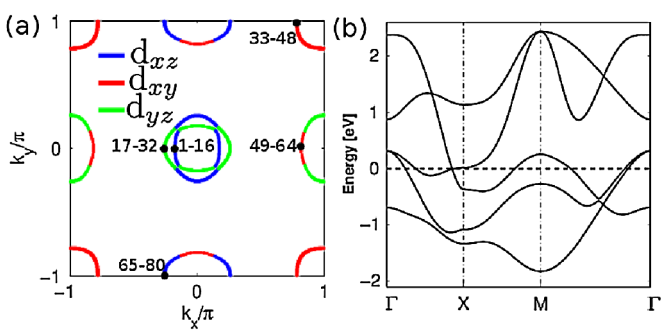


FIG. 1 (color online). (a) Schematic plot of the unfolded FS. (b) $k_z = 0$ slice of the 122 band structure given in Ref. [33]. The dominant orbital weights along the $e$ and $h$ pockets are highlighted in (a). The patches along pockets are enumerated counterclockwise, starting at each pocket with the patch indicated by a dot. The number of patches with electron pockets is 80, and without it decreases to 48.

A schematic picture of the FS topology is given in Fig. 1(a). The $h$ pockets at $\Gamma$ mainly have $d_{xz}$ and $d_{yz}$ orbital content, while the $h$ pocket at $M$ consists of $d_{xy}$ orbital weight. When present, the $e$ pockets consist of $d_{xz}$ and $d_{yz}$ orbital weight. Exceeding a certain size, the front tip along $\Gamma - X$ also has an important $d_{xy}$ weight on the $e$ pockets. We use the conventional on site orbital model for the interactions, i.e.,

$$H_{\text{int}} = \sum_i \Bigg[ U_1 \sum_a n_{i,a\uparrow} n_{i,a\downarrow} + U_2 \sum_{a<b,s,s'} n_{i,as} n_{i,bs'} + \sum_{a<b} \Bigg( J_H \sum_{s,s'} c^{\dagger}_{ias} c^{\dagger}_{ibs'} c_{ias'} c_{ibs} + J_{\text{pair}} c^{\dagger}_{ia\uparrow} c^{\dagger}_{ia\downarrow} c_{ib\downarrow} c_{ib\uparrow} \Bigg) \Bigg], \tag{2}$$

where $n_{i,as}$ denote density operators at site $i$ of spin $s$ in orbital $a$. We consider intra- and interorbital interactions $U_1$ and $U_2$ as well as Hund's coupling $J_H$ and pair hopping $J_{\text{pair}}$. We choose the values of the interaction parameters close to the ones obtained by constrained RPA *ab initio* calculations [34]: $U_1 > U_2 > J_H \sim J_{\text{pair}}$, and set $U_1 = 3.0$ eV, $U_2 = 2.0$ eV, and $J_H = J_{\text{pair}} = 0.6$ eV. While there are variations of these parameters for different classes of pnictides, the values of the parameters are all in the same range, and we have confirmed that variations of 20%–30% of the interaction parameters do not change the picture qualitatively. As a tendency, a comparably large absolute value of $U_1$ needs to be kept to trigger the SC instability, where increasing $U_2$ also helps to increase the critical cutoff scale and, thus, $T_c$.

Using the multiband FRG [9,35–37], we study the evolution of the renormalized interaction described by the 4-point function (4PF) under integrating out high energy fermionic modes: $V_\Lambda(\boldsymbol{k}_1;\boldsymbol{k}_2;\boldsymbol{k}_3;\boldsymbol{k}_4) c^{\dagger}_{\boldsymbol{k}_4 s} c^{\dagger}_{\boldsymbol{k}_3 \bar{s}} c_{\boldsymbol{k}_2 s} c_{\boldsymbol{k}_1 \bar{s}}$, where the flow parameter is the IR cutoff $\Lambda$ approaching the FS. $\boldsymbol{k}_1$–$\boldsymbol{k}_4$ are the incoming and outgoing momenta. The starting conditions are given by the bare initial interactions for the 4PF with the bandwidth serving as an UV cutoff. The diverging channels of the 4PF under the flow to the FS signal the nature of the instability, and the corresponding $\Lambda_c$ serves as an upper bound for the transition temperature $T_c$. The Cooper channel of the 4PF provides the different SC form factors—the dominant

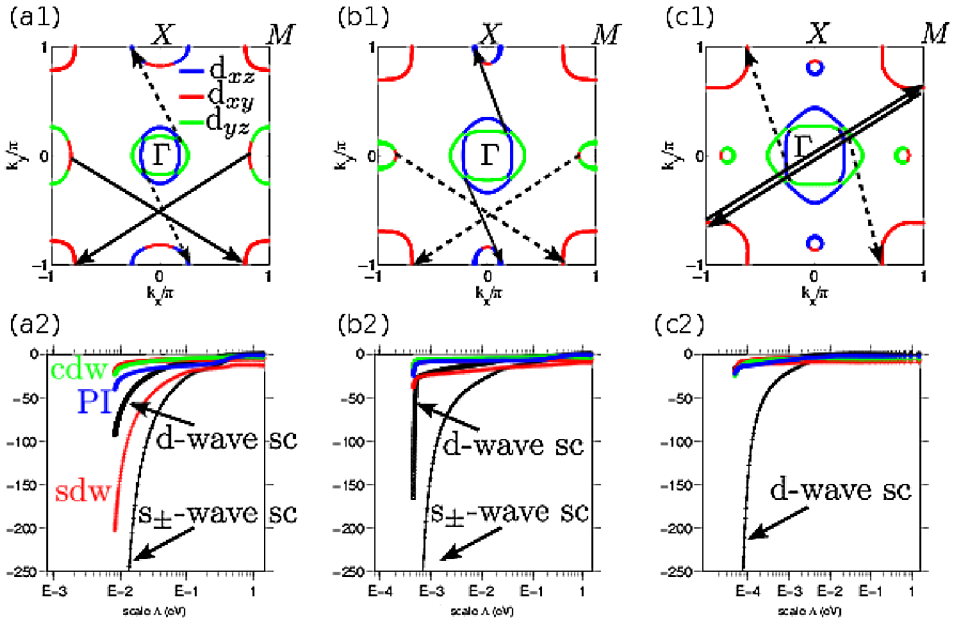


FIG. 2 (color online). Representative scenarios of the FS (unfolded Brillouin zone) and instability eigenvalue flows for chemical potential and electron concentration per iron $\mu = -0.12$, $n_{\rm el} = 5.913$ (a), $\mu = -0.22$, $n_{\rm el} = 5.663$ (b), and $\mu = -0.32$, $n_{\rm el} = 5.346$ in (c). The hole doping of our model calculation in (c), while exceeding the experimental setup $n_{\rm el} = 5.5$, best matches the FS profile from ARPES [32]. The dominant and subdominant scatterings in the Cooper channel are highlighted in (a1)–(c1) by full and dashed arrows. The color contours along the FS label the dominant orbital weights [inset (a1)]. The leading eigenvalue flow of the ordering channel for different Fermi instabilities [charge density wave (CDW), Pomeranchuk (PI), spin density wave (SDW), and superconductivity (SC)] are plotted in (a2)–(c2) versus the IR cutoff FRG flow parameter $\Lambda$. For (a) and (b) we find $s^{\pm}$ as the leading Fermi instability. For (c) we observe a leading $d$-wave instability.

order parameter having the largest eigenvalue [9,35–37]. In Fig. 2, the leading eigenvalues for different FS instabilities are plotted against $\Lambda$ for different fillings between moderately hole-doped from the left to strongly hole-doped to the right. We find that for all scenarios the leading instability is in the Cooper channel.

For the moderately doped case, the $e$ pockets are of similar size as the $h$ pockets. Figure 2(a1) shows the FS structure as well as the dominant (full line) and subdominant scattering (dashed arrow) processes in the Cooper channel. The two major components are given by $\Gamma \leftrightarrow X$ as well as $M \leftrightarrow X$ scatterings. They are particularly important for the front tips of the $e$ pockets since these parts can scatter to $M$ via dominant $U_1$ interaction due to identical orbital content. The spin-density wave (SDW) fluctuations are strong, signaling the proximity to the leading magnetic instability scenario of the undoped model [Fig. 2(a2)].

For the intermediate regime, between moderate and strong hole doping, the $e$ pockets are already very small [Fig. 2(b1)]. The nesting to the $h$ pocket is absent, and the SDW fluctuations are strongly reduced. In addition, the SDW fluctuations become less concentrated in the $(\pi, 0)/(0, \pi)$ or $(\pi, \pi)$ channel and spread into various incommensurate sectors [38]. The $d_{xy}$ orbital weight on the $e$ pocket is reduced, and the $M \leftrightarrow X$ scattering becomes subdominant. The main Cooper channel scattering is along $\Gamma \leftrightarrow X$. As a consequence, $s\pm$ is still the leading instability, where the form factor and its decomposition into orbital scattering contributions are shown in Fig. 3: The largest gap is found for the inner $h$ pocket at $\Gamma$, followed by the outer $h$ pocket and the $h$ pocket at $M$, where the $e$ pockets show anisotropic gaps. The orbital decomposition confirms the previous discussion of the dominant scattering contribution, in that the largest weight resides at intra- and interorbital scattering of the $d_{xz}$ and $d_{yz}$ orbital. However, we already observe that, due to the lack of SDW fluctuations supporting the SC, the critical divergence scale is decreased [Fig. 2]. In particular, while still subdominant, we can already see the $d$ wave evolving as the second-highest instability eigenvalue

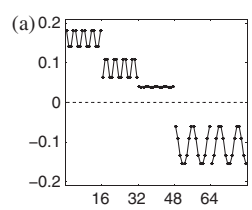


(b)

| $(a,b)$ | $d_{xz}$ | $d_{yz}$ | $d_{x^2-y^2}$ | $d_{xy}$ | $d_{3z^2-r^2}$ |
|---|---|---|---|---|---|
| $d_{xz}$ | -845.326 | -436.185 | -67.482 | -142.778 | -13.076 |
| $d_{yz}$ | -436.185 | -845.326 | -67.482 | -142.778 | -13.076 |
| $d_{x^2-y^2}$ | -67.482 | -67.482 | -33.036 | -27.675 | -5.542 |
| $d_{xy}$ | -142.778 | -142.778 | -27.675 | -87.978 | -6.087 |
| $d_{3z^2-r^2}$ | -13.076 | -13.076 | -5.542 | -6.087 | -1.558 |

FIG. 3. (a) Form factor of the leading SC instability of scenario Fig. 2(b), plotted versus the patching index of the Fermi pockets according to Fig. 1(a). (b) Eigenvalues of the orbital decomposition of the SC form factor in (a). The ratio of the values label the relative importance of the orbital scattering channel $V(a, a \to b, b) c_{a\uparrow} c_{a\downarrow} c^{\dagger}_{b\downarrow} c^{\dagger}_{b\uparrow}$.

in the Cooper channel. When $e$ pockets are still present, the form factor (not shown here) closely resembles the extended $d$-wave type involving $h$ pockets and $e$ pockets [36].

At strong hole doping, the $e$ pockets are absent, and the $h$ pockets are very large. The flow in Fig. 2(c) shows no instability up to small cutoff scales of $\Lambda$ where we find a leading instability in the Cooper channel. Its form factor and orbital scattering decomposition is shown in Fig. 4. We observe an extended $d$-wave instability on the three $h$ pockets, with nodes located along the main diagonals in the Brillouin zones [as seen by comparing the patch numbers of the 0 crossings in Fig. 4(a) and the patching enumeration defined in Fig. 1]. A harmonic analysis of the order parameter yields a large contribution of the $\cos(2k_x) - \cos(2k_y)$ type and a subdominant $\cos(k_x) - \cos(k_y)$ component; i.e., the form factor is most accurately characterized as $(\cos k_x + \cos k_y)(\cos k_x - \cos k_y)$. The dominant scattering is intrapocket scattering on the large $M$ $h$ pocket, followed by interorbital $d_{xy}$ to $d_{xz,yz}$ scattering between $M \leftrightarrow \Gamma$. While the magnetic fluctuations are generally weak in this regime, the dominant contribution is now given by $(\pi, \pi)$ SDW fluctuations as opposed to $(\pi, 0)/(\pi, 0)$ for smaller hole doping. For strong hole doping, the $h$ pocket at $M$ is large enough to induce higher harmonic $d$-wave SC through intrapocket scattering between the $d_{xy}$ orbitals as confirmed by the large value of $d_{xy} - d_{xy}$ pairing [Fig. 4(b)]. Via scattering to the other pockets, the SC instability is likewise induced there, however, with smaller amplitude than for the $M$ pocket [Fig. 4(a)]. As opposed to a conventional first harmonic $d$ wave, there is no sign change between the extended $d$-wave form factor on the $M$ pocket and the $\Gamma$ pocket according to $\cos(2k_x) - \cos(2k_y)$ [Fig. 4]. This picture of a $k$-space proximity effect from the $M$ pocket to the $\Gamma$ pockets is substantiated by our checks with calculations involving the $M$ pocket only, where we see a similar evolution of an SC instability (the divergence is lower, as the interorbital scatterings in the three pocket scenario help to renormalize the repulsive Coulomb interactions). This matches the orbital decomposition of the SC form factor in Fig. 4(b), showing dominant intraorbital scattering of the $d_{xy}$ orbital.

As apparent from the ARPES data, the nodal character of the SC phase in $KFe_2As_2$ cannot originate from possible nodes on the $e$ pockets (which are gapped out at these doping levels) but must be due to nodes on the $h$ pockets. It is then clear that the order parameter cannot be $s^{\pm}$ as it does not tend to allow for an anisotropy that would drive the $h$ pockets nodal. The $d$-wave instability which we find for the strongly hole-doped regime provides an explanation for the general experimental evidence, while the detailed gap structure certainly deserves further investigation [39]. Electron-phonon coupling may change the picture slightly quantitatively but not qualitatively, as the nodal features tentatively linked to the $d$-wave symmetry

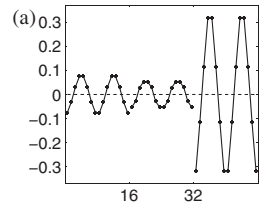


(b)

| $(a,b)$ | $d_{xz}$ | $d_{yz}$ | $d_{x^2-y^2}$ | $d_{xy}$ | $d_{3z^2-r^2}$ |
|---|---|---|---|---|---|
| $d_{xz}$ | -24.143 | -11.829 | -4.513 | -41.785 | -2.518 |
| $d_{yz}$ | -11.829 | -24.143 | -4.513 | -41.785 | -2.518 |
| $d_{x^2-y^2}$ | -4.513 | -4.513 | -3.798 | -23.405 | -1.412 |
| $d_{xy}$ | -41.785 | -41.785 | -23.405 | -567.184 | -23.598 |
| $d_{3z^2-r^2}$ | -2.518 | -2.518 | -1.412 | -23.598 | -1.721 |

FIG. 4. (a) Form factor of the leading SC instability of the strongly hole-doped scenario Fig. 2(c), plotted versus the patching index of the FS according to Fig. 1(a). (b) Eigenvalues of the orbital decomposition of the SC form factor in (a). We find a extended $d$-wave form factor. The nodal points are given along the main diagonal of the Brillouin zone; i.e., the form factor of the inner $h$ pocket, for example, crosses zero between the patches (2, 3), (6, 7), (10, 11), and (14, 15).

are unambiguously observed in the experiment. Pnictogen height variations as a function of doping may change the precise value of $T_c$ and would be important to be studied in general from first principles. Finally, it would be interesting to further analyze how the system evolves from the $s$-wave SC phase to the $d$-wave SC phase as a function of doping.

We thank A. Chubukov, H. Ding, S. Graser, D. van Harlingen, P. Hirschfeld, D. Scalapino, and Y.-L. Wu for discussions. R. T. and B. A. B. thank the IOP Beijing for hospitality, where some of the work has been done. We thank all participants of the KITP workshop "Iron-based superconductors" for discussions. We acknowledge computational resources by Reed College. R. T. is supported by the Humboldt Foundation. R. T. and C. P. are supported by DFG-SPP 1458/1 and C. P. by DFG-FOR 538. B. A. B. was supported by Sloan Foundation, NSF DMR-095242, NSF China 11050110420, and a MRSEC grant at Princeton University, NSF DMR-0819860.

[1] Y. Kamihara, T. Watanabe, M. Hirano, and H. Hosono, J. Am. Chem. Soc. **130**, 3296 (2008).
[2] K. Sasmal, B. Lv, B. Lorenz, A. M. Guloy, F. Chen, Y.-Y. Xue, and C.-W. Chu, Phys. Rev. Lett. **101**, 107007 (2008).
[3] K. Seo, B. A. Bernevig, and J. Hu, Phys. Rev. Lett. **101**, 206404 (2008).
[4] I. I. Mazin, D. J. Singh, M. D. Johannes, and M. H. Du, Phys. Rev. Lett. **101**, 057003 (2008).
[5] A. V. Chubukov, D. V. Efremov, and I. Eremin, Phys. Rev. B **78**, 134512 (2008).
[6] V. Stanev, J. Kang, and Z. Tesanovic, Phys. Rev. B **78**, 184509 (2008).
[7] T. A. Maier, S. Graser, D. J. Scalapino, and P. J. Hirschfeld, Phys. Rev. B **79**, 224510 (2009).
[8] K. Kuroki, H. Usui, S. Onari, R. Arita, and H. Aoki, Phys. Rev. B **79**, 224511 (2009).
[9] R. Thomale, C. Platt, W. Hanke, and B. A. Bernevig, Phys. Rev. Lett. **106**, 187003 (2011).
[10] K. Hashimoto, T. Shibauchi, S. Kasahara, K. Ikada, S. Tonegawa, T. Kato, R. Okazaki, C. J. van der Beek,

M. Konczykowski, H. Takeya, K. Hirata, T. Terashima, and Y. Matsuda, Phys. Rev. Lett. **102**, 207001 (2009).

[11] L. Malone, J. D. Fletcher, A. Serafin, A. Carrington, N. D. Zhigadlo, Z. Bukowski, S. Katrych, and J. Karpinski, Phys. Rev. B **79**, 140501 (2009).

[12] M. A. Tanatar, J.-Ph. Reid, H. Shakeripour, X. G. Luo, N. Doiron-Leyraud, N. Ni, S. L. Bud'ko, P. C. Canfield, R. Prozorov, and L. Taillefer, Phys. Rev. Lett. **104**, 067002 (2010).

[13] J. G. Checkelsky, L. Li, G. F. Chen, J. L. Luo, N. L. Wang, and N. P. Ong, arXiv:0811.4668.

[14] M. Yamashita, N. Nakata, Y. Senshu, S. Tonegawa, K. Ikada, K. Hashimoto, H. Sugawara, T. Shibauchi, and Y. Matsuda, Phys. Rev. B **80**, 220509 (2009).

[15] C. W. Hicks, T. M. Lippman, M. E. Huber, J. G. Analytis, J.-H. Chu, A. S. Erickson, I. R. Fisher, and K. A. Moler, Phys. Rev. Lett. **103**, 127003 (2009).

[16] G. Xu, H. Zhang, X. Dai, and Z. Fang, Europhys. Lett. **84**, 67 015 (2008).

[17] W. Hanke, C. Platt, and R. Thomale, Ann. Phys. (Berlin) **523**, 638 (2011).

[18] Y. J. Yan, X. F. Wang, R. H. Liu, H. Chen, Y. L. Xie, J. J. Ying, and X. H. Chen, Phys. Rev. B **81**, 235107 (2010).

[19] N. Ni, S. L. Bud'ko, A. Kreyssig, S. Nandi, G. E. Rustan, A. I. Goldman, S. Gupta, J. D. Corbett, A. Kracher, and P. C. Canfield, Phys. Rev. B **78**, 014507 (2008).

[20] G. F. Chen, Z. Li, J. Dong, G. Li, W. Z. Hu, X. D. Zhang, X. H. Song, P. Zheng, N. L. Wang, and J. L. Luo, Phys. Rev. B **78**, 224512 (2008).

[21] C. Martin, R. T. Gordon, M. A. Tanatar, H. Kim, N. Ni, S. L. Bud'ko, P. C. Canfield, H. Luo, H. H. Wen, Z. Wang, A. B. Vorontsov, V. G. Kogan, and R. Prozorov, Phys. Rev. B **80**, 020501 (2009).

[22] X. G. Luo, M. A. Tanatar, J.-Ph. Reid, H. Shakeripour, N. Doiron-Leyraud, N. Ni, S. L. Bud'ko, P. C. Canfield, H. Luo, Z. Wang, H.-H. Wen, R. Prozorov, and L. Taillefer, Phys. Rev. B **80**, 140503 (2009).

[23] M. Rotter, M. Tegel, and D. Johrendt, Phys. Rev. Lett. **101**, 107006 (2008).

[24] L. Wray, D. Qian, D. Hsieh, Y. Xia, L. Li, J. G. Checkelsky, A. Pasupathy, K. K. Gomes, C. V. Parker, A. V. Fedorov, G. F. Chen, J. L. Luo, A. Yazdani, N. P. Ong, N. L. Wang, and M. Z. Hasan, Phys. Rev. B **78**, 184508 (2008).

[25] H. Ding, P. Richard, K. Nakayama, K. Sugawara, T. Arakane, Y. Sekiba, A. Takayama, S. Souma, T. Sato, T. Takahashi, Z. Wang, X. Dai, Z. Fang, G. F. Chen, J. L. Luo, and N. L. Wang, Europhys. Lett. **83**, 47 001 (2008).

[26] Y. Zhang, L. X. Yang, F. Chen, B. Zhou, X. F. Wang, X. H. Chen, M. Arita, K. Shimada, H. Namatame, M. Taniguchi, J. P. Hu, B. P. Xie, and D. L. Feng, Phys. Rev. Lett. **105**, 117003 (2010).

[27] J. K. Dong, S. Y. Zhou, T. Y. Guan, H. Zhang, Y. F. Dai, X. Qiu, X. F. Wang, Y. He, X. H. Chen, and S. Y. Li, Phys. Rev. Lett. **104**, 087005 (2010).

[28] T. Terashima, M. Kimata, N. Kurita, H. Satsukawa, A. Harada, K. Hazama, M. Imai, A. Sato, K. Kihou, C.-H. Lee, H. Kito, H. Eisaki, A. Iyo, T. Saito, H. Fukazawa, Y. Kohori, H. Harima, and S. Uji, Phys. Rev. Lett. **104**, 259701 (2010).

[29] K. Hashimoto, A. Serafin, S. Tonegawa, R. Katsumata, R. Okazaki, T. Saito, H. Fukazawa, Y. Kohori, K. Kihou, C. H. Lee, A. Iyo, H. Eisaki, H. Ikeda, Y. Matsuda, A. Carrington, and T. Shibauchi, Phys. Rev. B **82**, 014526 (2010).

[30] H. Fukazawa, Y. Yamada, K. Kondo, T. Saito, Y. Kohori, K. Kuga, Y. Matsumoto, S. Nakatsuji, H. Kito, P. M. Shirage, K. Kihou, N. Takeshita, C.-H. Lee, A. Iyo, and H. Eisaki, J. Phys. Soc. Jpn. **78**, 083712 (2009).

[31] S. W. Zhang, L. Ma, Y. D. Hou, J. Zhang, T.-L. Xia, G. F. Chen, J. P. Hu, G. M. Luke, and W. Yu, Phys. Rev. B **81**, 012503 (2010).

[32] T. Sato, K. Nakayama, Y. Sekiba, P. Richard, Y.-M. Xu, S. Souma, T. Takahashi, G. F. Chen, J. L. Luo, N. L. Wang, and H. Ding, Phys. Rev. Lett. **103**, 047002 (2009).

[33] S. Graser, A. F. Kemper, T. A. Maier, H.-P. Cheng, P. J. Hirschfeld, and D. J. Scalapino, Phys. Rev. B **81**, 214503 (2010).

[34] T. Miyake, K. Nakamura, R. Arita, and M. Imada, J. Phys. Soc. Jpn. **79**, 044705 (2010).

[35] F. Wang, H. Zhai, Y. Ran, A. Vishwanath, and D.-H. Lee, Phys. Rev. Lett. **102**, 047005 (2009).

[36] R. Thomale, C. Platt, J. Hu, C. Honerkamp, and B. A. Bernevig, Phys. Rev. B **80**, 180505 (2009).

[37] C. Platt, C. Honerkamp, and W. Hanke, New J. Phys. **11**, 055058 (2009).

[38] C. H. Lee, K. Kihou, H. Kawano-Furukawa, T. Saito, A. Iyo, H. Eisaki, H. Fukazawa, Y. Kohori, K. Suzuki, H. Usui, K. Kuroki, and K. Yamada, Phys. Rev. Lett. **106**, 067003 (2011).

[39] H. Kawano-Furukawa, C. J. Bowell, J. S. White, R. W. Heslop, A. S. Cameron, E. M. Forgan, K. Kihou, C. H. Lee, A. Iyo, H. Eisaki, T. Saito, H. Fukazawa, Y. Kohori, R. Cubitt, C. D. Dewhurst, J. L. Gavilano, and M. Zolliker, Phys. Rev. B **84**, 024507 (2011).